

Three-dimensional higher-spin Dirac and Weyl dispersions in the strongly-isotropic K_4 crystal

Masahisa Tsuchiizu

Department of Physics, Nagoya University, Nagoya 464-8602, Japan

(Dated: September 30, 2016)

We analyze the electronic structure in the three-dimensional (3D) crystal formed by the sp^2 hybridized orbitals (K_4 crystal), by the tight-binding approach based on the first-principles calculation. We discover that the bulk Dirac-cone dispersions are realized in the K_4 crystal. In contrast to the graphene, the energy dispersions of the Dirac cones are isotropic in 3D and the pseudospin $S = 1$ Dirac cones emerge at the Γ and H points of the bcc Brillouin zone, where three bands become degenerate and merge at a single point belonging to the T_2 irreducible representation. In addition, the usual $S = 1/2$ Dirac cones emerge at the P point. By focusing the hoppings between the nearest-neighbor sites, we show an analytic form of the tight-binding Hamiltonian with a 4×4 matrix, and we give an explicit derivation of the $S = 1$ and $S = 1/2$ Dirac-cone dispersions. We also analyze the effect of the spin-orbit coupling to examine how the degeneracies at Dirac points are lifted. At the $S = 1$ Dirac points, the spin-orbit coupling lifts the energy level with six-fold degeneracy into two energy levels with two-dimensional \bar{E}_2 and the four-dimensional \bar{F} representations. Remarkably, all the dispersions near the \bar{F} point show the linear dependence in the momentum with different velocities. We derive the effective Hamiltonian near the \bar{F} point and find that the band contact point is described by the $S = 3/2$ Weyl point.

PACS numbers: 71.20.Gj, 31.15.aq, 73.22.Pr

I. INTRODUCTION

Electronic structure of graphene has been a subject of intensive research over the years [1–4], since it has been recognized as the most exciting material after to the discovery of the massless Dirac fermions [5, 6]. The massless Dirac fermions have been widely recognized in the condensed-matter systems, especially in the context of the topological insulators [7, 8]. In the case of graphene, the sp^2 hybridized orbitals build up the honeycomb crystal, and the π electrons exhibit the Dirac fermion behavior on it. Recently, the 3D analogue of the graphene has also attracted much attention [9, 10]. Even in the 3D diamond structure, the suppression of the density of states has been observed in the valence band [11] and the possible realization of the three-dimensional (3D) Dirac cone has been discussed [9].

From the mathematical point of view, the honeycomb and the diamond crystals have the common properties, called the *strongly-isotropic* property [12, 13]. The strongly-isotropic property indicates the property that preserves the crystal net after any permutation of bonds with common end point. The honeycomb structure is the only crystal that possesses the strongly-isotropic property. In 3D, there are only two strongly-isotropic crystals: one is the diamond crystal and the other is the K_4 crystal. The K_4 crystal is defined as the standard realization of the maximal topological crystal over the K_4 graph [12, 13]. Here K_4 represents the complete graph with four vertices, as shown in Fig. 1(a), and its crystal structure is shown in Fig. 1(b). Like the 2D honeycomb crystal, the coordination number of the K_4 crystal is three. The synthesis of the K_4 crystal in terms of the carbon atoms (called the K_4 carbon) has not been succeeded so far despite the several theoretical predictions based on the first-principles calculations [14, 15]. Quite recently, the discovery of the K_4 crystal was made where the constituting unit is a large molecule instead of the carbon atom [16].

The effect of the spin-orbit coupling (SOC) on the Dirac

cones has been attracting great interest owing to the discovery of the topological insulator [17]. In the case of honeycomb structure, the degeneracy of the Dirac point is lifted and the gap appears. On the other hand, in the case of diamond crystal, the SOC lifts the degeneracy along the X - W line in the Brillouin zone [9] except for the X point, i.e., the two bands touch at the X point. Due to the presence of the inversion (I) and time-reversal (TR) symmetries, each band is doubly degenerate at general \mathbf{k} points and thus the contact point has four-fold degeneracy. Thus the band touching point at the X point is the Dirac point, which is described by the four-band Dirac Hamiltonian. If the I or TR symmetry is broken, the double degeneracy at general \mathbf{k} points is lifted. In this case, the possibility of the low-symmetry band touchings has been argued [18, 19], where the contact point has two-fold degeneracy.

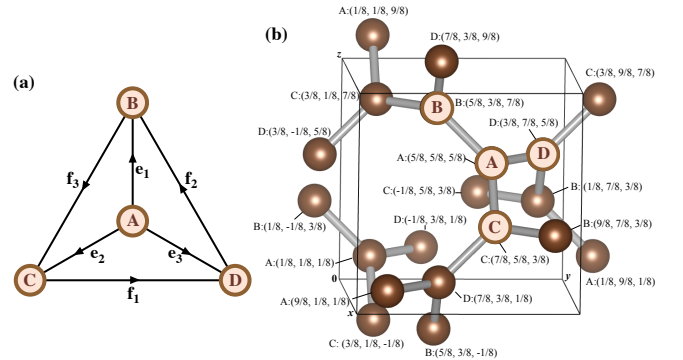


FIG. 1: (Color online) (a) The complete graph K_4 where $\{A, B, C, D\}$ are the vertices and $\{e_1, e_2, e_3, f_1, f_2, f_3\}$ are the oriented edges. (b) The K_4 crystal structure. The numbers in the parentheses represent the fractional Cartesian coordinates in the cubic conventional unit cell. There are eight sites in the conventional unit cell. In the primitive unit cell, there are four sites, A, B, C, and D. The coordination number is three and the bonds connecting nearest-neighbor sites are represented by the vectors given in Eq. (1).

acy. These touching points are referred to as the Weyl points [20, 21]. Recently, the experimental realization of the Weyl points has been reported [22].

In the present paper, we analyze the band structure of the K_4 crystal by the tight-binding approach. We discover that three-dimensional Dirac-cone dispersions are realized in the K_4 crystal. In contrast to the graphene, three bands touch at a single point on the Γ and H points of the bcc Brillouin zone, indicating the emergence of pseudospin $S = 1$ Dirac cone. In addition, the usual $S = 1/2$ Dirac cones emerge at the P point, where the two bands touch at a single point. Since the I symmetry is broken in the K_4 crystal, the energy splitting due to SOC is peculiar. We show that, at the $S = 1$ Dirac points, the SOC lifts the energy level with six-fold degeneracy into two energy levels with two-dimensional \bar{E}_2 and the four-dimensional \bar{F} irreducible representations. Especially, we find that the dispersion near the \bar{F} point is described by the $S = 3/2$ Weyl dispersions.

The present paper is organized as follows. In Sec. II, we recall briefly how the K_4 crystal can be realized from the the K_4 graph and how the strongly-isotropic character is retained. In Sec. III, we construct the tight-binding model for the K_4 carbon based on the first-principles calculation by focusing on the carbon π orbital. In Sec. IV, the tight-binding Hamiltonian is analyzed and we show explicitly how the pseudospin $S = 1$ and $S = 1/2$ Dirac-cone dispersions are derived. Finally, in Sec. V, the effect of the SOC is analyzed. Section VI is devoted to the summary and discussions.

II. K_4 CRYSTAL

The K_4 crystal is realized as the maximal topological crystal over the K_4 graph. The general arguments to obtain the realization of the crystal from the finite graph are based on the homology group. Here, we simply follow the algorithm given in Refs. [12] and [13] to construct of the K_4 crystal, without the mathematical details. In the graph K_4 of Fig. 1(a), the vertices are described by $\{A, B, C, D\}$ and the edges are $\{e_1, e_2, e_3, f_1, f_2, f_3\}$. First we consider three closed paths $c_1 = (e_2, f_1, \bar{e}_3)$, $c_2 = (e_3, f_2, \bar{e}_1)$, $c_3 = (e_1, f_3, \bar{e}_2)$ in the K_4 graph [Fig. 1(a)]. The inner product can be introduced by $\langle e, e' \rangle = 1$ (if $e' = e$), -1 (if $e' = \bar{e}$), and 0 (otherwise), where $e, e' = e_i, f_i$. Then we find $|c_1|^2 = |c_2|^2 = |c_3|^2 = 3$ and $\langle c_i, c_j \rangle = -1$ ($i \neq j$). The vectors connecting the nearest-neighbor sites (building blocks) for the infinite K_4 crystal, $\mathbf{v}(e_i)$ and $\mathbf{v}(f_i)$, can be constructed by taking c_1, c_2, c_3 as the basis, e.g., $\mathbf{v}(e_1) = a_1 \mathbf{c}_1 + a_2 \mathbf{c}_2 + a_3 \mathbf{c}_3$ ($a_i \in \mathbb{R}$). From the relations $\langle \mathbf{v}(e_1), c_1 \rangle = \langle e_1, c_1 \rangle = 0$, $\langle \mathbf{v}(e_1), c_2 \rangle = \langle e_1, c_2 \rangle = -1$, and $\langle \mathbf{v}(e_1), c_3 \rangle = \langle e_1, c_3 \rangle = +1$, we can obtain $a_1 = 0$, $a_2 = -1/4$, and $a_3 = +1/4$, and thus $\mathbf{v}(e_1)$ is determined as $\mathbf{v}(e_1) = -\mathbf{c}_2/4 + \mathbf{c}_3/4$. From this simple calculation, we can get the following relations:

$$\begin{aligned}\mathbf{v}(e_1) &= -\frac{1}{4}\mathbf{c}_2 + \frac{1}{4}\mathbf{c}_3, \\ \mathbf{v}(e_2) &= -\frac{1}{4}\mathbf{c}_3 + \frac{1}{4}\mathbf{c}_1,\end{aligned}$$

$$\begin{aligned}\mathbf{v}(e_3) &= -\frac{1}{4}\mathbf{c}_1 + \frac{1}{4}\mathbf{c}_2, \\ \mathbf{v}(f_1) &= +\frac{1}{2}\mathbf{c}_1 + \frac{1}{4}\mathbf{c}_2 + \frac{1}{4}\mathbf{c}_3, \\ \mathbf{v}(f_2) &= +\frac{1}{2}\mathbf{c}_2 + \frac{1}{4}\mathbf{c}_3 + \frac{1}{4}\mathbf{c}_1, \\ \mathbf{v}(f_3) &= +\frac{1}{2}\mathbf{c}_3 + \frac{1}{4}\mathbf{c}_1 + \frac{1}{4}\mathbf{c}_2,\end{aligned}\tag{1}$$

The vectors $\pm \mathbf{v}(e_i)$ and $\pm \mathbf{v}(f_i)$ constitute the building block of the K_4 crystal, e.g., $\mathbf{v}(e_1)$ is the vector connecting the A and B sites in Fig. 1(b).

One possible choice of \mathbf{c}_i as $\mathbf{c}_1 = (+1, -1, -1)$, $\mathbf{c}_2 = (-1, +1, -1)$, and $\mathbf{c}_3 = (-1, -1, +1)$. The realized K_4 crystal is shown in Fig. 1(b). The numbers in the parentheses represent the fractional Cartesian coordinates in the cubic conventional unit cell, where we note that the lattice constant becomes $a = 2$ by the definition of the building block vectors [Eq. (1)]. From the crystallographic point of view, the space group of the K_4 crystal is $I4_132$ (No. 214) and the primitive vectors are chosen as $\mathbf{t}_1 = (-\frac{1}{2}, \frac{1}{2}, \frac{1}{2})$, $\mathbf{t}_2 = (\frac{1}{2}, -\frac{1}{2}, \frac{1}{2})$, and $\mathbf{t}_3 = (\frac{1}{2}, \frac{1}{2}, -\frac{1}{2})$, in the unit $a = 2$. There are four sites in the primitive cell and these four sites are specified as A, B, C, and D, in Fig. 1. The coordination number is three, as in the 2D graphene.

The K_4 crystal has the remarkable mathematical property, called the *strongly-isotropic* property [12, 13], indicating the property that preserves the crystal net after any permutation of bonds with common end point. For example, by focusing of the A site at $(\frac{1}{8}, \frac{1}{8}, \frac{1}{8})$ in Fig. 1(b), we can keep the crystal net even if we exchange the bonds $\mathbf{v}(e_2)$ and $\mathbf{v}(e_3)$ while the $\mathbf{v}(e_1)$ bond is fixed. This congruent transformation can be realized by combination of the rotation about the two-fold rotation axis C_{2f} [23] and the subsequent translation $\mathbf{r} \rightarrow \mathbf{r} + \mathbf{t}$ where $\mathbf{t} = (\frac{1}{4}, \frac{1}{4}, \frac{1}{4})$. In the usual crystallographic notation, this transformation is represented by $\{C_{2f}|\frac{1}{2}\frac{1}{2}\frac{1}{2}\}$, which is nothing but one element of the space group $I4_132$. Here, we note that the translation vector $\frac{1}{2}\frac{1}{2}\frac{1}{2}$ is given in the unit of the primitive vectors, i.e., $\mathbf{t} = \frac{1}{2}\frac{1}{2}\frac{1}{2} = \frac{1}{2}\mathbf{t}_1 + \frac{1}{2}\mathbf{t}_2 + \frac{1}{2}\mathbf{t}_3 = (\frac{1}{4}, \frac{1}{4}, \frac{1}{4})$. It is known that the honeycomb and the diamond crystals have this strongly-isotropic property [12, 13]. The honeycomb is the only crystal having the strongly-isotropic property in 2D, and there are only two strongly-isotropic crystals in 3D: one is the diamond crystal and the other is the K_4 crystal. In this sense, the diamond crystal and K_4 crystal are the most *beautiful* crystals in 3D and the K_4 crystal can be called the *diamond twin* [13]. It has been emphasized [12, 13] that the K_4 crystal has chirality as can be seen from the existence of the 4_1 screw axis, in contrast to the diamond crystal. Thus the effect of the SOC on the K_4 crystal is different from that on the diamond crystal due to the lack of the I symmetry. We argue the effect of the SOC in Sec. V.

III. K_4 CARBON

In this section, we construct the tight-binding model for the K_4 carbon in terms of the first-principles calculation.

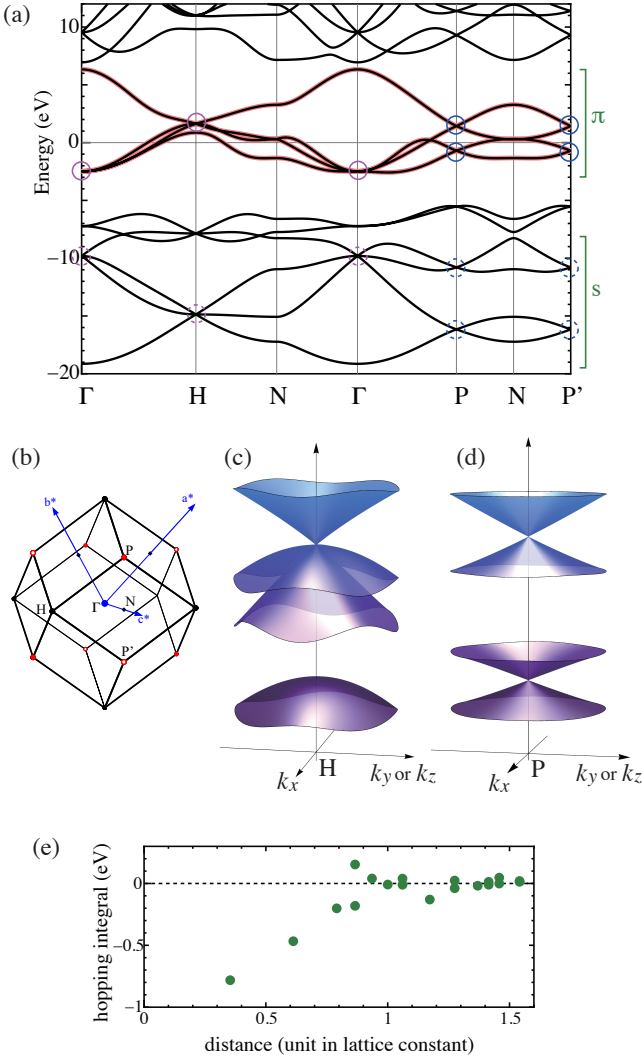


FIG. 2: (Color online) (a) The band structure for the K_4 carbon obtained from the first-principles calculation. The band structure by the tight-binding model is shown by the bold (red) curves. (b) The Brillouin zone for bcc. The band structures near the H (c) and P (d) points. (e) The evaluated hopping integrals as a function of the intersite distance.

A. Band structure of the K_4 carbon

The stability of the K_4 carbon has been discussed theoretically and the metallic behavior was predicted [14, 15]. The optimized bond distance is $1.4 - 1.5$ Å, which is comparable to that in diamond and graphite. Figure 2(a) shows the band structure obtained by the first-principles density-functional-theory (DFT) calculation based on generalized gradient approximation with the use of the WIEN2k code [24]. The lattice constant is set as $a = 4.063$ Å, according to Ref. [14], where the bond distances for nearest-neighbor sites is $d \approx 1.44$ Å. The Brillouin zone is shown in Fig. 2(b). The band structure well reproduce the ones reported in Refs. 14 and 15. The four conduction bands in the energy range $-3.5 \text{ eV} < E_k < 6.5 \text{ eV}$ are constructed by the carbon p

orbitals that stand perpendicular to the plane formed by the nearest-neighbor carbon atoms, i.e., by the “ π ” orbitals. The valence bands in the energy range $-20 \text{ eV} < E_k \lesssim -8 \text{ eV}$ are mainly formed by the carbon s orbitals. The bands at $-8 \text{ eV} \lesssim E_k < -5 \text{ eV}$ are constructed by both the s orbitals and the p orbitals elongated perpendicular to the π orbital, i.e., by the “ σ ” hybridized orbitals. We observe two kinds of the nontrivial degenerate points in the conduction bands. First, at the H (Γ) point, the bands are triply degenerate with $E = 1.63$ eV (-2.48 eV). The band structure near the H point is explicitly shown in Fig. 2(c). We find that the bands near the H point exhibit the linear k dependencies except for the middle band. Due to the 3D isotropic structure, the band structures are isotropic with the axes k_x , k_y , and k_z . Secondly, a pairs of the degenerate two bands can be observed at the P point, as shown in Fig. 2(d). We also note that the triply and doubly degenerate points can also be observed in the valence bands.

B. Tight-binding model of the K_4 carbon

In order to analyze the band structure in more detail, we construct the tight-binding model based on the maximally localized Wannier functions [25], by targeting the four conduction bands in the energy range $-3.5 \text{ eV} < E_k < 6.5 \text{ eV}$. The Wannier functions contributing these four bands are well described by the π orbitals. The standing directions of the π orbitals for the A - D sites can be described by the normal vectors $\mathbf{n}(A) = (1, 1, 1)$, $\mathbf{n}(B) = (-1, 1, 1)$, $\mathbf{n}(C) = (1, -1, 1)$, and $\mathbf{n}(D) = (1, 1, -1)$. These four π orbitals in the primitive unit cell construct four conduction bands. The tight-binding hopping integrals evaluated on the basis of the Wannier functions [25] are shown in Fig. 2(e). The hopping parameter for the nearest neighbor sites is given by $t_1 = -0.782$ eV. This parameter can be contrasted to the one in the graphene [26, 27]: Recent evaluation of the hopping parameters for 2D graphene indicates $(pp\pi) \approx -3.0$ eV [27]. The hopping amplitude depends on the angle between the π orbitals of the neighboring carbon atoms. In terms of the Slater-Koster parameterization [28], the nearest-neighbor hopping integral for the K_4 carbon is given by $t_1 = (pp\pi)/3$. Thus the parameter of $(pp\pi)$ for the K_4 carbon is consistent with that for the graphene. In addition, we observe that the amplitudes of the long-distance hoppings are relatively large. This fact is also consistent with the results in the graphene [27].

The band structures obtained from the tight-binding approximation are shown by bold (red) curves in Fig. 2(a). We find the tight-binding model based only on the π orbital perfectly reproduces the DFT results of the conduction bands. There is presumably small but nonzero hopping between the π and s orbitals with different sites. Such an effect would be included effectively and, as a result, the relatively large long-distance hopping parameters are obtained. This would be one reason why the four π -orbital description works well.

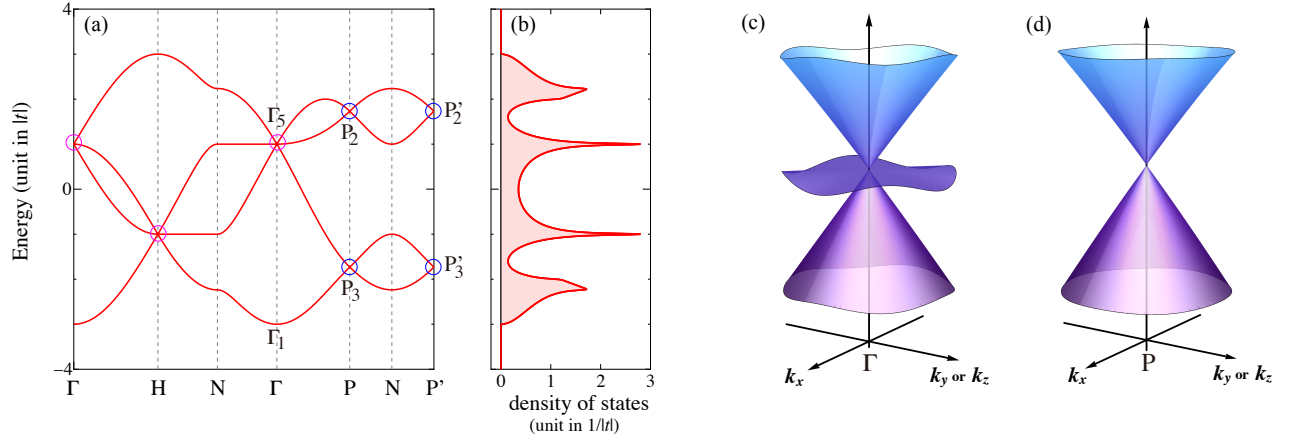


FIG. 3: (Color online) (a) The band structures of the tight-binding model for the K_4 crystal. Only the nearest-neighbor hoppings are taken into account. The Dirac points are indicated by circles. The triple degeneracy at the Γ_5 point is described by the three-dimensional real T_2 irreducible representation, and the double degeneracies at the P_2 and P_3 points are described by the two-dimensional complex 1F_2 and 1F_3 irreducible representations. The P_2 and P'_2 (P_3 and P'_3) are the conjugate pair of the complex representation. (b) The density of states. The case for half filling $n = 1$ is shown where n is the filling factor. The Fermi energy coincides with that of the $S = 1$ Dirac point if $n = 2/3$ or $4/3$. (c) The $S = 1$ Dirac cone at the Γ and H points. (d) The $S = 1/2$ Dirac cone at the P points.

IV. DIRAC POINTS IN THE K_4 CRYSTAL

In the section, we analyze the Γ and P points on the basis of the tight-binding model and show that the degenerate points at Γ and P points are described by the pseudospin $S = 1$ and $S = 1/2$ Dirac cones, respectively. A generalization of the Dirac cone structure to possess pseudospin $S > \frac{1}{2}$ has been discussed in the literature [29–31]. In the conventional $S = 1/2$ Dirac cone, *two* bands exhibit linear dependence in the momentum and touch at a single point. In contrast, in the $S = 1$ case, *three* bands become degenerate and touch at a single point, where anomalous physical behavior can be expected [31]. Recently a possible system to emerge the $S = 1$ Dirac cone has been proposed in terms of the first-principles calculation [32]. However, the explicit tight-binding model that exhibits the $S = 1$ Dirac cone is not obtained, and then the physical properties have not been clarified yet.

In order to simplify the discussions, we focus on the nearest-neighbor hopping only. This situation is indeed relevant to the recently-discovered K_4 crystal [16], as will be discussed later. Since there are four sites in the primitive unit cell, the Hamiltonian can be described as the 4×4 matrix in the orbital basis $(\varphi_A(\mathbf{k}), \varphi_B(\mathbf{k}), \varphi_C(\mathbf{k}), \varphi_D(\mathbf{k}))$. Here we consider the s -orbital bands. The tight-binding Hamiltonian is explicitly given by

$$H_{\mathbf{k}} = - \begin{pmatrix} 0 & e^{-\frac{i}{2}\mathbf{k}\cdot\mathbf{v}(e_1)} & e^{-\frac{i}{2}\mathbf{k}\cdot\mathbf{v}(e_2)} & e^{-\frac{i}{2}\mathbf{k}\cdot\mathbf{v}(e_3)} \\ e^{\frac{i}{2}\mathbf{k}\cdot\mathbf{v}(e_1)} & 0 & e^{-\frac{i}{2}\mathbf{k}\cdot\mathbf{v}(f_3)} & e^{\frac{i}{2}\mathbf{k}\cdot\mathbf{v}(f_2)} \\ e^{\frac{i}{2}\mathbf{k}\cdot\mathbf{v}(e_2)} & e^{\frac{i}{2}\mathbf{k}\cdot\mathbf{v}(f_3)} & 0 & e^{-\frac{i}{2}\mathbf{k}\cdot\mathbf{v}(f_1)} \\ e^{\frac{i}{2}\mathbf{k}\cdot\mathbf{v}(e_3)} & e^{-\frac{i}{2}\mathbf{k}\cdot\mathbf{v}(f_2)} & e^{\frac{i}{2}\mathbf{k}\cdot\mathbf{v}(f_1)} & 0 \end{pmatrix}. \quad (2)$$

Owing to the property of completeness of K_4 , the off-diagonal components of the matrix become dense. The nearest-neighbor hopping parameter is set to $t = -1$. The building block vectors [Eq. (1)] are explicitly given by $\mathbf{v}(e_1) =$

$\frac{1}{2}(0, -1, 1)$, $\mathbf{v}(e_2) = \frac{1}{2}(1, 0, -1)$, $\mathbf{v}(e_3) = \frac{1}{2}(-1, 1, 0)$, $\mathbf{v}(f_1) = \frac{1}{2}(0, -1, -1)$, $\mathbf{v}(f_2) = \frac{1}{2}(-1, 0, -1)$, and $\mathbf{v}(f_3) = \frac{1}{2}(-1, -1, 0)$. In the s -orbital case, the sign of the hopping is common. If we consider the π -orbital case, the sign of the hopping integral can be altered depending on bonding or anti-bonding character of the π overlapping. The signs of the hoppings are determined by those of the inner product of vectors, i.e., $\mathbf{n}(B) \cdot \mathbf{n}(C) = -1$, $\mathbf{n}(B) \cdot \mathbf{n}(D) = -1$, $\mathbf{n}(C) \cdot \mathbf{n}(D) = -1$, and become positive otherwise. Thus in the case of π -orbital case the extra prefactor -1 should be added for the (2,3), (2,4), (3,2), (3,4), (4,2), (4,3) matrix components.

The band structures obtained from Eq. (2) are shown in Fig. 3(a). The degenerate dispersion relations near the Γ and H points (P and P' points) can be described by the $S = 1$ ($S = 1/2$) Dirac cone as shown shortly. The $S = 1$ Dirac point is at the Γ_5 point with the energy $E = +1$ where the bands are triply degenerate. The triple degeneracy at the Γ_5 point is described by the three-dimensional real T_2 irreducible representation [23]. The same profile can be seen at the H point. The $S = 1/2$ Dirac points are at P_2 and P_3 points where the bands are doubly degenerate at the energy $E = \pm\sqrt{3}$. The double degeneracies at P_2 and P_3 are described by the two-dimensional complex 1F_2 and 1F_3 irreducible representations [23]. Due to the presence of the flat bands near the $S = 1$ Dirac points at Γ and H , the critical enhancement can be observed at $E = \pm 1$ in density of states (DOS), as shown in Fig. 3(c). In contrast, sufficient suppressions can be seen at $E = \pm\sqrt{3}$, reflecting the presence of the $S = 1/2$ Dirac cones. The same profile of the DOS can be seen in the 3D hyperkagomé crystal except for the van Hove singularity owing to flat bands [33]. Note that the DOS does not vanish precisely at $E = \pm\sqrt{3}$, since another band across this energy at different position in \mathbf{k} .

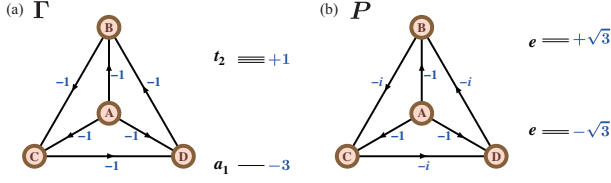


FIG. 4: (Color online) The structure of the Hamiltonian matrix and the corresponding energy diagrams at the Γ point (a) and the P point (b).

A. $S = 1$ Dirac cone at the Γ point

Here we derive the effective Hamiltonian near the Γ point and show explicitly that its character is described by pseudospin $S = 1$ Dirac cone. By setting $\mathbf{k} = (0, 0, 0)$ in Eq. (2), all the off-diagonal matrix elements become -1 , and then the eigenvalues are -3 (no degeneracy) and $+1$ (triple degeneracy) [see Fig. 4(a)]. The energy separation at the Γ point can be recognized by regarding the K_4 graph [Fig. 1(a)] as a regular tetrahedron. The eigenfunctions of the regular tetrahedron can be classified according to the representation of the point group T_d and are composed of the A_1 representation and the T_2 representation. In the tight-binding picture, the A_1 representation has the energy -3 and the T_2 representation have $+1$. One of the possible choice of the unitary matrix for diagonalizing $H_{\mathbf{k}}$ on the Γ point is given by

$$U_{\Gamma} = \frac{1}{2} \begin{pmatrix} 1 & e^{-i\frac{\pi}{4}} & e^{+i\frac{\pi}{2}} & e^{+i\frac{\pi}{4}} \\ 1 & e^{-i\frac{3\pi}{4}} & e^{-i\frac{\pi}{2}} & e^{+i\frac{3\pi}{4}} \\ 1 & e^{+i\frac{\pi}{4}} & e^{-i\frac{\pi}{2}} & e^{-i\frac{\pi}{4}} \\ 1 & e^{+i\frac{3\pi}{4}} & e^{+i\frac{\pi}{2}} & e^{-i\frac{3\pi}{4}} \end{pmatrix}. \quad (3)$$

The first column corresponds to the A_1 representation and the remaining three columns to the T_2 representation of the point group T_d . By applying this unitary matrix to the Hamiltonian (2), and by expanding the momentum up to $O(k)$, we obtain

$$U_{\Gamma}^{\dagger} H_{\mathbf{k}} U_{\Gamma} = \hat{E}_{\Gamma} + \frac{1}{2} \begin{pmatrix} 0 & 0 & 0 & 0 \\ 0 & k_z & \frac{1}{\sqrt{2}}k_{-} & 0 \\ 0 & \frac{1}{\sqrt{2}}k_{+} & 0 & \frac{1}{\sqrt{2}}k_{-} \\ 0 & 0 & \frac{1}{\sqrt{2}}k_{+} & -k_z \end{pmatrix} + O(k^2), \quad (4)$$

where $k_{\pm} \equiv (k_x \pm ik_y)$, and $\hat{E}_{\Gamma} = \text{diag}(-3, 1, 1, 1)$ is the set of the energy eigenvalues on the Γ point. If we focus on the second, third, and fourth rows and columns in the second term in Eq. (4), the effective Hamiltonian is given by the 3×3 matrix:

$$H_{\text{eff}} = \frac{1}{2} \mathbf{k} \cdot \mathbf{S}, \quad (5)$$

where $\mathbf{S} = (S_x, S_y, S_z)$ is the spin-1 matrix:

$$S_x = \begin{pmatrix} 0 & \frac{1}{\sqrt{2}} & 0 \\ \frac{1}{\sqrt{2}} & 0 & \frac{1}{\sqrt{2}} \\ 0 & \frac{1}{\sqrt{2}} & 0 \end{pmatrix}, \quad S_y = \begin{pmatrix} 0 & \frac{-i}{\sqrt{2}} & 0 \\ \frac{i}{\sqrt{2}} & 0 & \frac{-i}{\sqrt{2}} \\ 0 & \frac{i}{\sqrt{2}} & 0 \end{pmatrix},$$

$$S_z = \begin{pmatrix} 1 & 0 & 0 \\ 0 & 0 & 0 \\ 0 & 0 & -1 \end{pmatrix}. \quad (6)$$

Thus the electronic structure near the Γ point is described by the pseudospin $S = 1$ Dirac cone. The energy dispersions are given by

$$\begin{aligned} E_{\mathbf{k}}^{+} &= 1 + \frac{1}{2} \sqrt{k_x^2 + k_y^2 + k_z^2} + O(k^2), \\ E_{\mathbf{k}}^0 &= 1 + O(k^2), \\ E_{\mathbf{k}}^{-} &= 1 - \frac{1}{2} \sqrt{k_x^2 + k_y^2 + k_z^2} + O(k^2). \end{aligned} \quad (7)$$

The dispersion relations near the H point are described in a similar manner. The $S = 1$ Dirac cone structure near the Γ_5 point is shown in Fig. 3(c).

B. $S = \frac{1}{2}$ Dirac cone at the P point

Next, we focus on the dispersion relations near the P point. By setting $\mathbf{k} = \mathbf{P} \equiv (\pi, \pi, \pi)$ in Eq. (2), some matrix elements become imaginary [see Fig. 4(b)] and the eigenvalues are $\pm\sqrt{3}$ with double degeneracy. We find that the conjugate pair of the eigenfunctions $(\varphi_A, \varphi_B, \varphi_C, \varphi_D) = (0, 1, \omega, \omega^2)$ and $(0, 1, \omega^2, \omega)$, where $\omega \equiv \exp(i2\pi/3)$, have different energies. The degenerate pairs can be generated by the C_2 transformation of the regular tetrahedron, e.g., $(A, B, C, D) \rightarrow (C, iD, A, -iB)$. Then the full eigenfunctions are $(\varphi_A, \varphi_B, \varphi_C, \varphi_D) = (0, 1, \omega, \omega^2)$ and $(\omega, i\omega^2, 0, -i)$ for $E_{\mathbf{k}} = +\sqrt{3}$, and $(\varphi_A, \varphi_B, \varphi_C, \varphi_D) = (0, 1, \omega^2, \omega)$ and $(\omega^2, i\omega, 0, -i)$ for $E_{\mathbf{k}} = -\sqrt{3}$. From the Gram-Schmidt orthogonalization procedure, one of the choices of the unitary matrix for diagonalizing $H_{\mathbf{k}}$ on the P point is given by

$$U_P = \frac{1}{\sqrt{6}} \begin{pmatrix} \sqrt{3} & 0 & -\sqrt{3} & 0 \\ 1 & \sqrt{2} & 1 & \sqrt{2}\omega^2 \\ 1 & \sqrt{2}\omega & 1 & \sqrt{2}\omega \\ 1 & \sqrt{2}\omega^2 & 1 & \sqrt{2} \end{pmatrix}. \quad (8)$$

The first and second (third and fourth) columns represent the eigenvectors for the eigenvalue $+\sqrt{3}(-\sqrt{3})$. In order to analyze the dispersion relation near this point, we apply the unitary transformation to the Hamiltonian (2). By expanding it up to the first order in the momentum \mathbf{k} , we find

$$U_P^\dagger H_{P+\mathbf{k}} U_P = \hat{E}_P + \frac{1}{6} \begin{pmatrix} k_x + k_y + k_z & \sqrt{2}(k_x + \omega^2 k_y + \omega k_z) & k_x + k_y + k_z & -\frac{1}{\sqrt{2}}(\omega^2 k_x + k_y + \omega k_z) \\ & -(k_x + k_y + k_z) & -\frac{1}{\sqrt{2}}(k_x + \omega k_y + \omega^2 k_z) & -(\omega^2 k_x + \omega k_y + k_z) \\ & & k_x + k_y + k_z & \sqrt{2}(\omega^2 k_x + k_y + \omega k_z) \\ & & & -(k_x + k_y + k_z) \end{pmatrix} + O(k^2), \quad (9)$$

where $\hat{E}_P = \text{diag}(-\sqrt{3}, -\sqrt{3}, +\sqrt{3}, +\sqrt{3})$ is the set of the energy eigenvalues on the P point. Here the quantity \mathbf{k} indicates the momentum centered at the P point. From the perturbative arguments up to $O(k_i)$, we can neglect the off-diagonal matrix elements connecting the states with different eigenvalues $\pm\sqrt{3}$, since the contributions of the dropped terms are of the order of k^2 . Thus the Hamiltonian (9) can be divided into two 2×2 Hamiltonians. The effective Hamiltonian representing lower two bands is given by

$$H_{\mathbf{k}}^{\text{eff}} = \frac{1}{6} \begin{pmatrix} k_x + k_y + k_z & \sqrt{2}(k_x + \omega^2 k_y + \omega k_z) \\ \sqrt{2}(k_x + \omega k_y + \omega^2 k_z) & -k_x - k_y - k_z \end{pmatrix}, \quad (10)$$

From this Hamiltonian, we immediately find that the energy dispersion is given by

$$E_{\mathbf{k},\pm}^{\text{eff}} = \pm \frac{1}{2\sqrt{3}} \sqrt{k_x^2 + k_y^2 + k_z^2} + O(k^2), \quad (11)$$

which represents the 3D $S = 1/2$ Dirac cone. The dispersion relation near the P point is shown in Fig. 3(d). In the case of the P' point, the Dirac cone has opposite chirality, as in the case of 2D graphene.

In the above analysis, we focused only on the nearest-neighbor hopping. By taking into account the long-distance hopping parameters shown in Fig. 2(e), the conduction π band dispersions can be reproduced [the bold (red) curves in Fig. 2(a)]. We find that the Dirac cone structures are robust against the long-distance hoppings. Here we note that, in the case of the π orbital, the structures at Γ and H points are interchanged. Since the long-distance hopping parameters are relatively large, the band structures are strongly modified. Especially, the energy level with the A_1 representation (Γ_1 point) becomes higher than that of the $S = 1/2$ Dirac point at the P_3 point in the case of the carbon system. However, in the case of the recently-discovered K_4 crystal [16], the long-distance hopping can be small and this simple treatment based only on the nearest-neighbor hopping can be justified, as will be discussed later.

V. EFFECT OF THE SPIN-ORBIT COUPLING

In this section, we analyze the effect of the SOC in the K_4 crystal. The effect of the SOC is not common even within the strongly-isotropic crystals. The Dirac points in the 2D graphene are not robust against the SOC [17], on the other hand, the Dirac points can emerge in 3D diamond as a consequence of the SOC [9]. In contrast to the 2D honeycomb and

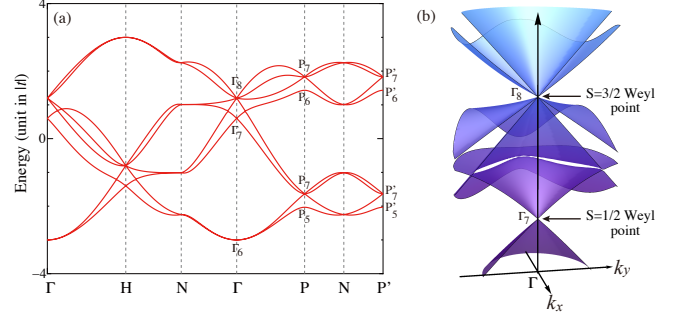


FIG. 5: (Color online) (a) The band structure of the tight-binding model for the K_4 crystal with the spin-orbit interaction $\lambda_{\text{SO}} = 0.05$. In the double-valued representation, the Γ_6 and Γ_7 points are described by the two-dimensional \bar{E}_1 and \bar{E}_2 irreducible representation, respectively, and the Γ_8 point is by the four-dimensional \bar{F} representation. The P_5 and P_6 points are the conjugate pair of the one-dimensional $^1\bar{E}$ and $^2\bar{E}$ representation. The triple degeneracy at the P_7 points is described by the three-dimensional \bar{T} representation. (b) The dispersions near the Γ_7 and Γ_8 point are shown with fixed $k_z = 0$. In this figure, only the region $k_x < 0$ is shown.

3D diamond crystals, the K_4 crystal does not hold the inversion symmetry [12]. Thus the degeneracy of band at general points is lifted due to the SOC, and the modification of the band structure near the Dirac points shows unique properties.

As has been discussed in Refs. [7, 9, 17], the intrinsic SOC can be expressed in terms of spin-dependent next-nearest-neighbor hopping. The explicit Hamiltonian of the SOC is given by

$$H_{\text{SOC}} = i \frac{8\lambda_{\text{SO}}}{a^2} \sum_{\langle\langle ij \rangle\rangle} c_i^\dagger \mathbf{s} \cdot (\mathbf{v}_{ij}^1 \times \mathbf{v}_{ij}^2) c_j, \quad (12)$$

where $\langle\langle ij \rangle\rangle$ represents the summation of the sites over the next-nearest neighbor pairs, and $\mathbf{v}_{ij}^{1,2}$ are the nearest neighbor bond vectors traversed between sites i and j . The band structure of the tight-binding model (2) in the presence of the SOC term (12) is shown in Fig. 5(a). In the general points of \mathbf{k} , the degeneracy of the bands is lifted due to the SOC since the K_4 crystal does not have the inversion symmetry.

The band structures near the Γ point show unique properties. When the SOC is introduced, the six-fold degeneracy at the Γ_5 point splits into two energy levels of $E_{\Gamma_7} = +1 - 8\lambda_{\text{SO}}$ with the two-dimensional Γ_7 (\bar{E}_2) representation and $E_{\Gamma_8} = +1 + 4\lambda_{\text{SO}}$ with the four-dimensional Γ_8 (\bar{F}) representation, whereas the Γ_1 point turns into the two-dimensional Γ_6 (\bar{E}_1) with the energy $E_{\Gamma_6} = -3$. The effective Hamiltonian near the Γ point can be obtained by applying the transformation given

by Eq. (3) to the SOC term [Eq. (12)]. Especially near the $S = 1$ Dirac point (Γ_5), the SOC induces an perturbation in the form of a 6×6 matrix:

$$H_{\text{SOC}}^{\text{eff}} = 4\lambda_{\text{SO}} \mathbf{S} \cdot \boldsymbol{\sigma}, \quad (13)$$

where $\boldsymbol{\sigma} = (\sigma_x, \sigma_y, \sigma_z)$ is the 2×2 Pauli matrix representing the electron's spin. The energy dispersion near the Γ_7 and Γ_8 points is shown in Fig. 5(b). Near the four-fold degenerate Γ_8 point, the band structure exhibits the linear \mathbf{k} dependencies. The effective Hamiltonian near the Γ_8 point can be derived by considering the situation $|\mathbf{k}| \ll |\lambda_{\text{SO}}|$ and is described by a 4×4 matrix. By applying an appropriate unitary transformation for diagonalizing the SOC term, the effective Hamiltonian is given by $H_{\Gamma_8}^{\text{eff}} = 1 + 4\lambda_{\text{SO}} + \frac{1}{3}\mathbf{k} \cdot \mathbf{J}$, where $\mathbf{J} = (J_x, J_y, J_z)$ is the 4×4 spin-3/2 matrix. Therefore the dispersions near the Γ_8 point are described by the $S = 3/2$ Weyl dispersions, where the dispersions take forms $1 + 4\lambda_{\text{SO}} \pm \frac{1}{2}|\mathbf{k}|$ and $1 + 4\lambda_{\text{SO}} \pm \frac{1}{6}|\mathbf{k}|$. Incidentally, we can observe $S = 1/2$ Weyl dispersions around the Γ_7 point, where the energy dispersions are given by $1 - 8\lambda_{\text{SO}} \pm \frac{1}{3}|\mathbf{k}|$. Similar structure can be observed at the H point.

At the P point, we also observe the unique properties. The energy splitting on the P points are given by $\pm\sqrt{3} - 6\lambda_{\text{SO}}$ (unique) at the P_5 or P_6 point and $\pm\sqrt{3} + 2\lambda_{\text{SO}}$ (triply degenerate) at the P_7 point. The P_5 and P_6 points are described by the conjugate pair of the one-dimensional complex $^1\bar{E}$ and $^2\bar{E}$ representations. On the other hand, the P_7 point is described by the \bar{T} representation and would be described by the $S = 1$ Weyl point. Incidentally, we observe several contact points with accidental degeneracy at general \mathbf{k} points, e.g., along the Γ - P and Γ - N lines. Analyses of physical quantities on this system are desired for future work.

VI. SUMMARY

In summary, we have examined the energy dispersion of the K_4 crystal in detail. The tight-binding model has been derived explicitly where we show the emergence of the pseudospin $S = 1$ and $S = 1/2$ Dirac cones. We have also analyzed the effect of SOC to examine how the degeneracies at the Dirac points are lifted. In contrast to the other strongly-isotropic honeycomb and diamond crystals, the K_4 crystal lacks the inversion symmetry, and the lowering of the symmetry is quite peculiar. We found that, by including the SOC, the $S = 1$ Dirac point split into the $S = 3/2$ Weyl point with the four-dimensional \bar{F} representation and the $S = 1/2$ Weyl point

with the two-dimensional \bar{E}_2 representation.

Here we note the magnitude of the SOC in the K_4 carbon system. In the Sec. V, we have analyzed the SOC based on the tight-binding model. It is well known that the SOC is small in the carbon system because of the light atom. We have performed the first-principles calculation to the K_4 carbon system, including the SOC. We have verified that the energy splitting given in Fig. 5 can be reproduced from the first-principles calculation, but the energy splitting of the six-fold degeneracy at the H point is small ~ 10 meV. As has been discussed in Ref. [9], the replacement of carbon atoms with heavier atoms enlarges the energy splitting. Further physical and chemical analyses are necessary for the realization of $S = 3/2$ Weyl semimetal in the K_4 crystal, i.e., for clarifying the conditions that the $S = 3/2$ Weyl point emerges at the Fermi energy without the other Fermi surfaces.

Finally we briefly discuss the relevance of the present analysis to the recently-synthesized K_4 crystal. The first success in synthesizing the K_4 crystal was achieved [16], where the constituting component is a molecule (called the NDI- Δ), instead of the carbon atom. In this material, the frontier molecular orbitals are extended along the neighboring molecules, i.e., the inter-molecular overlapping is of the σ type. In addition, the long distance hoppings are not relevant since the distance between the next-nearest-neighbor molecules is large ($= \sqrt{3}/8a \sim 18$ Å). Thus the dispersive band structure is similar to that shown in Fig. 3(a). In addition, the filling factor n for the NDI- Δ system, was evaluated as $n \approx 1.4$ [16], which is close to $n = 4/3$. This indicates a possibility that the Fermi energy lies on the $S = 1$ Dirac point, i.e., the $S = 1$ Dirac semimetal. Additionally, nontrivial flat bands have been pointed out reflecting the peculiar molecular structure of NDI- Δ [16]. Further theoretical investigation needed for analyzing the electronic states in the newly-discovered K_4 crystal is left for future work.

Acknowledgments

The author is thankful for fruitful discussions with K. Awaga, M. M. Matsushita, Y. Shuku, A. Mizuno, R. Suizu, V. Robert, A. Kobayashi, and A. Yamakage. This work was supported by Grant-in-Aid for Scientific Research (24740232, 25400370, and 16K05442) from the Ministry of Education, Culture, Sports, Science and Technology, Japan, and Japan-France Integrated Action Program, from Japan Society for the Promotion of Science.

-
- [1] T. Ando, in *Nano-Physics & Bio-Electronics: A New Odyssey*, edited by T. Chakraborty, F. Peeters, and U. Sivan (Elsevier, Amsterdam, 2002), pp. 1–64.
 - [2] D. S. L. Abergel, V. Apalkov, J. Berashevich, K. Ziegler, and T. Chakraborty, *Adv. Phys.* **59**, 261 (2010).
 - [3] H. Aoki and M. S. Dresselhaus, eds., *Physics of Graphene*, NanoScience and Technology (Springer International Publish-

- ing, Switzerland, 2014).
- [4] J. Inoue, A. Yamakage, and S. Honda, *Graphene in Spintronics: Fundamentals and Applications* (CRC Press, 2016).
- [5] P. R. Wallace, *Phys. Rev.* **71**, 622 (1947).
- [6] J. C. Slonczewski and P. R. Weiss, *Phys. Rev.* **109**, 272 (1958).
- [7] L. Fu, C. L. Kane, and E. J. Mele, *Phys. Rev. Lett.* **98**, 106803 (2007).

- [8] M. Z. Hasan and C. L. Kane, *Rev. Mod. Phys.* **82**, 3045 (2010).
- [9] S. M. Young, S. Zaheer, J. C. Y. Teo, C. L. Kane, E. J. Mele, and A. M. Rappe, *Phys. Rev. Lett.* **108**, 140405 (2012).
- [10] B.-J. Yang and N. Nagaosa, *Nat. Comms.* **5**, 4898 (2014).
- [11] D. J. Chadi and M. L. Cohen, *Phys. Status Solidi B* **68**, 405 (1975).
- [12] T. Sunada, *Notices of the AMS* **55**, 208 (2007).
- [13] T. Sunada, *Topological Crystallography With a View Towards Discrete Geometric Analysis* (Springer, 2013).
- [14] G. M. Rignanes and J. C. Charlier, *Phys. Rev. B* **78**, 125415 (2008).
- [15] M. Itoh, M. Kotani, H. Naito, T. Sunada, Y. Kawazoe, and T. Adachi, *Phys. Rev. Lett.* **102**, 055703 (2009).
- [16] A. Mizuno, Y. Shuku, R. Suizu, M. M. Matsushita, M. Tsuchizu, D. Reta Mañeru, F. Illas, V. Robert, and K. Awaga, *J. Am. Chem. Soc.* **137**, 7612 (2015).
- [17] C. L. Kane and E. J. Mele, *Phys. Rev. Lett.* **95**, 226801 (2005).
- [18] G. B. Halász and L. Balents, *Phys. Rev. B* **85**, 035103 (2012).
- [19] J. Liu and D. Vanderbilt, *Phys. Rev. B* **90**, 155316 (2014).
- [20] X. Wan, A. M. Turner, A. Vishwanath, and S. Y. Savrasov, *Phys. Rev. B* **83**, 205101 (2011).
- [21] A. A. Burkov and L. Balents, *Phys. Rev. Lett.* **107**, 127205 (2011).
- [22] L. Lu, Z. Wang, D. Ye, L. Ran, L. Fu, J. D. Joannopoulos, and M. Soljačić, *Science* **349**, 622 (2015).
- [23] C. J. Bradley and A. P. Cracknell, *The Mathematical Theory of Symmetry in Solids: Representation Theory for Point Groups and Space Groups* (Clarendon Press., Oxford, 1972).
- [24] P. Blaha, K. Schwarz, G. Madsen, D. Kvasnicka, and J. Luitz, *WIEN2k, An Augmented Plane Wave + Local Orbitals Program for Calculating Crystal Properties* (Karlheinz Schwarz, Techn. Universitt Wien, Austria, 2001).
- [25] J. Kuneš, R. Arita, P. Wissgott, A. Toschi, H. Ikeda, and K. Held, *Comput. Phys. Commun.* **181**, 1888 (2010).
- [26] S. Reich, J. Maultzsch, C. Thomsen, and P. Ordejón, *Phys. Rev. B* **66**, 035412 (2002).
- [27] J. Jung and A. H. MacDonald, *Phys. Rev. B* **87**, 195450 (2013).
- [28] J. C. Slater and G. F. Koster, *Phys. Rev.* **94**, 1498 (1954).
- [29] H. Watanabe, Y. Hatsugai, and H. Aoki, *J. Phys.: Conf. Ser.* **334**, 012044 (2011).
- [30] M. Orlita, D. M. Basko, M. S. Zholudev, F. Teppe, W. Knap, V. I. Gavrilenco, N. N. Mikhailov, S. A. Dvoretzkii, P. Neugebauer, C. Faugeras, et al., *Nat. Phys.* **10**, 233 (2014).
- [31] J. D. Malcolm and E. J. Nicol, *Phys. Rev. B* **90**, 035405 (2014).
- [32] G. Giovannetti, M. Capone, J. van den Brink, and C. Ortix, *Phys. Rev. B* **91**, 121417 (2015).
- [33] M. Udagawa and Y. Motome, *J. Phys.: Conf. Ser.* **145**, 012013 (2009).